Radiation Characteristics of *Chlamydomonas reinhardtii* CC125 and Its Truncated Chlorophyll Antenna Transformants *tla1*, *tlaX*, and *tla1-CW*$^{+}$

Halil Berberoglu[*], Laurent Pilon[*,§] and Anastasios Melis[†]

[*]Mechanical and Aerospace Engineering Department
Henry Samueli School of Engineering and Applied Science
University of California, Los Angeles - Los Angeles, CA 90095, USA
[§] Corresponding Author
Phone: +1 (310)-206-5598, Fax: +1 (310)-206-4830
E-mail: pilon@seas.ucla.edu

[†]Department of Plant and Microbial Biology
University of California, Berkeley, - Berkeley, CA 94720, USA

November 15, 2008

ABSTRACT

This experimental study reports, for the first time, the radiation characteristics of the unicellular green algae *Chlamydomonas reinhardtii* strain CC125 and its truncated chlorophyll antenna transformants *tla1*, *tlaX*, and *tla1-CW*$^{+}$. Photobiological hydrogen production is a sustainable alternative to thermo-chemical and electrolytic technologies with the possible advantage of carbon dioxide mitigation. However, scale-up of photobioreactors from bench top to industrial scale is made difficult by excessive absorption and waste of light energy as heat and fluorescence. This results in limited light penetration into the photobioreactor and low solar to hydrogen energy conversion efficiency. To overcome these challenges, the algae *Chlamydomonas reinhardtii* have been genetically engineered with reduced pigment concentrations in their photosystems. This can improve the performance of photobioreactors by increasing the saturation irradiance of algae and quantum efficiency of photobiological hydrogen production.

The extinction and absorption coefficients of all strains studied are obtained from normal-normal and normal-hemispherical transmittance measurements over the spectral range from 300 to 1,300 nm. Moreover, a polar nephelometer is used to measure the scattering phase function of the microorganisms at 632.8 nm. It is established that the wild strain *C.reinhardtii* CC125 has major absorption peaks at 435 and 676 nm, corresponding to the in vivo absorption peaks of chlorophyll *a*, and at 475 and 650 nm corresponding to those of chlorophyll *b*. The genetically engineered strains have less chlorophyll pigments than the wild strain and thus have smaller absorption cross-sections. In particular, the mutant *tlaX* features a significant reduction in chlorophyll *b* concentration. For all mutants, however the reduction in the absorption cross-section is accompanied by an increase in scattering cross-section. Although scattering becomes the dominant phenomenon contributing to the overall extinction of light, it is mainly in the forward direction. Thus, to fully assess the effect of genetic engineering on light transport in the photobioreactor requires careful radiation transfer analysis using the radiation characteristics reported in this study.

NOMENCLATURE

a	scattering particle diameter, [m]
$A_{abs,\lambda}$	spectral mass absorption cross-section, [m^2kg^{-1}]
$E_{ext,\lambda}$	spectral mass extinction cross-section, [m^2kg^{-1}]
f_1	weighing factor in TPF
g	Henyey-Greenstein asymmetry factor
h_1	weighing factor in TPF
I	radiance (intensity), [$Wm^{-2}sr^{-1}$]
L	coordinate direction, Figure 4(b)
l_p	photon path length, [m]
n	refractive index
OD	optical density
P	pathlength, $P = w/2sin\Theta + r$
r	the radius of rotation of the fiber-optic probe, [m]
$\hat{s}$	local spatial coordinate unit vector
$S_{sca,\lambda}$	spectral mass scattering cross-section of microorganisms, [m^2kg^{-1}]
t	sample thickness, [m]
T	transmittance, [%]
U	correction term in recovering the phase function, Equation (12)
w	incident beam diameter, [m]
X	microorganism concentration, [kgm^{-3}]
x	size parameter
z	distance between the detector and the virtual image of the last lens, [m]

Greek symbols

β	extinction coefficient, [m^{-1}]
ϵ_h	contribution of the forward scattered light to $T_{h,\lambda,X}$
ϵ_n	contribution of the forward scattered light to $T_{\lambda,X}$
Θ	scattering angle, [rad]
Θ_a	half acceptance angle of the detector, [rad]
κ	absorption coefficient, [m^{-1}]
λ	wavelength, [nm]
Ω	solid angle, [sr]
σ	scattering coefficient, [m^{-1}]
τ	nondimensional optical thickness
Φ	scattering phase function
χ	apparent(uncorrected) extinction coefficient, [m^{-1}]
χ_h	apparent(uncorrected) absorption coefficient, [m^{-1}]

Subscripts

λ	refers to wavelength
h	refers to normal-hemispherical measurements
HG	refers to Henyey-Greenstein phase function
PBS	refers to phosphate buffer saline solution
TPF	refers to truncated phase function

1 INTRODUCTION

Photobioreactors are enclosures used for cultivating microorganisms that utilize sunlight as their energy source for their growth and subsequent product formation [1]. They have been used in environmental engineering such as wastewater treatment, heavy metal removal, and CO_2 mitigation [2]. More recently, they have also been considered for hydrogen production [3–7]. In photobiological hydrogen production, the presence of dissolved O_2 in the liquid medium and limited sunlight penetration through a high density culture are the major issues limiting the solar energy conversion efficiency [8–12]. The former has been alleviated by reversibly shutting down the O_2 production metabolism of the unicellular green algae *Chlamydomonas reinhardtii* by sulphur deprivation [13]. This establishes *C.reinhardtii* as one of the best candidates for photobiological hydrogen production [8,9,13]. However, limited solar radiation penetration remains a challenge affecting the H_2 production rate and the solar to H_2 energy conversion efficiency of high density mass cultures.

Solar radiation transfer within absorbing, scattering, and non-emitting media, such as microorganism suspensions in photobioreactors, is governed by the radiative transport equation (RTE) [14]. The RTE is a semi-empirical integro-differential equation derived from energy conservation considerations. For a given wavelength λ, it is expressed in terms of dimensionless optical coordinates as [15],

$$\frac{\mathrm{d}I_\lambda}{\mathrm{d}\tau_\lambda} = -I_\lambda(\tau_\lambda, \hat{s}) + \frac{\omega_\lambda}{4\pi}\int_{4\pi} I_\lambda(\tau_\lambda, \hat{s}_i)\Phi_\lambda(\hat{s}_i, \hat{s})d\Omega_i \tag{1}$$

where I_λ is the spectral radiance (sometimes known as spectral intensity [15]) expressed in $\mathrm{Wm^{-2}sr^{-1}}$. Here, $\hat{s}$ is the unit vector in the line-of-sight direction and $d\Omega_i$ is the solid angle around $\hat{s}_i$. The dimensionless optical thickness τ_λ and the single scattering albedo ω_λ are defined, respectively, as

$$\tau_\lambda = \int_0^s (\kappa_\lambda + \sigma_\lambda)ds = \int_0^s \beta_\lambda ds \tag{2}$$

$$\text{and} \qquad \omega_\lambda = \frac{\sigma_\lambda}{\kappa_\lambda + \sigma_\lambda} = \frac{\sigma_\lambda}{\beta_\lambda} \tag{3}$$

where κ_λ, σ_λ, and β_λ $(= \kappa_\lambda + \sigma_\lambda)$ are the absorption, scattering, and extinction coefficients, respectively and expressed in $\mathrm{m^{-1}}$. The scattering phase function $\Phi_\lambda(\hat{s}_i, \hat{s})$ represents the probability that the radiation propagating in direction $\hat{s}_i$ be scattered in direction $\hat{s}$, and is normalized such that

$$\frac{1}{4\pi}\int_{4\pi} \Phi_\lambda(\hat{s}_i, \hat{s})d\Omega_i = 1 \tag{4}$$

Note that the variables κ_λ, σ_λ, β_λ, and Φ_λ are often denoted by a_λ, b_λ, c_λ, and β_λ, respectively, in the ocean optics literature [16–18]. In the present study, the nomenclature commonly used in the radiative heat transfer community is employed [15].

Equation (1) indicates that the absorption and scattering coefficients, or the extinction coefficient and the single scattering albedo, together with the scattering phase function are major parameters needed to solve the radiation transfer equation and predict light transfer in photobioreactors for simulation, design and optimization purposes. However, these

characteristics are strongly dependent on wavelength and difficult to predict from electromagnetic wave theory given the complex morphology of the microorganisms and their various chromophores.

Moreover, wild type strains of algae found in nature contain more light harvesting pigments than necessary for the saturation of photosynthesis under bright sunlight, which is a survival strategy due to limited light in their natural habitats [19]. However, this is disadvantageous in scaled-up photobioreactors because (i) the algae close to the light source will absorb more light than they can utilize and waste it and (ii) light will not penetrate deep into the photobioreactor resulting in a reduction of the system efficiency. In order to overcome these challenges, Polle *et al.* [19] genetically engineered the green algae *Chlamydomonas reinhardtii* to have less pigments by truncating their chlorophyll antenna size. The authors demonstrated that the saturation irradiance of photosynthesis was increased by approximately a factor 2 from about 1,500 to 3,000 μmol/m^2/s.

Qualitatively, the genetic transformation is apparent to the unaided eye as the genetically engineered strains appear light green while the wild strain appears dark green. This study aims at quantitatively assessing the effect of genetic engineering on the radiation characteristics of *C.reinhardtii* CC125 and its truncated chlorophyll antenna transformants *tla1*, *tlaX*, and *tla1*-CW$^+$.

2 CURRENT STATE OF KNOWLEDGE

Truncated Chlorophyll Antenna Transformants

Photochemical reactions conducted by algae start with the absorption of solar light by the pigments in the light harvesting chlorophyll antenna complexes [20]. Besides having a chlorophyll *a* containing core antenna complex, *C.reinhardtii* also has a chlorophyll *b* containing auxiliary light-harvesting antenna [20]. These complexes channel the solar energy to two distinct photosystems, namely photosystem I and II (PSI and PSII), where electrons necessary for driving various chemical reactions are generated from oxidation of water [21]. In *C.reinhardtii* wild strain, PSI and PSII are reported to contain 240 and 230 chlorophyll molecules, respectively [8]. However, for proper functioning of these complexes under bright sunlight, the algae need only 95 and 37 chlorophyll molecules in the core complexes of PSI and PSII, respectively [13]. Polle *et al.* [20] genetically engineered *C.reinhardtii* via DNA insertional mutagenesis to obtain the mutant strain *tla1* having permanently reduced number of chlorophyll molecules per photosystem. This strain was derived from a cell wall-less strain CC425-CW$^-$ and did not contain cell wall [20]. For use in photobioreactors it is necessary that cells have walls so that they do not break upon mechanical stirring [20]. Thus, Polle *et al.* [20] crossed *tla1* with a cell wall containing strain CC1068 and isolated the strain *tla1*-CW$^+$ showing observable characteristics (phenotype) of *tla1* and having a cell wall. The strain CC125 is the wild type *C.reinhardtii* and is used as a reference to compare the radiation characteristics of the genetically engineered strains. Finally, the strain *tlaX* has even a smaller chlorophyll antenna than *tla1*. At the time of preparation of the manuscript no publications were available on the mutant *tlaX*. The reduction in pigment concentration compared with *tla1* is evident to the naked eye.

Measurement of the Radiation Characteristics

The radiation characteristics of microorganisms are measured under the single scattering regime [22]. This means that the scattered light undergoes only one scattering event in the sample. This condition is satisfied if the sample thickness t is much smaller than the photon mean free path l_p such that [23, 24],

$$t(1 - g_\lambda) \ll l_{p,\lambda} \tag{5}$$

where $l_{p,\lambda} = 1/\beta_\lambda$ and g_λ is the mean cosine of the scattering angle. The latter is also known as the Henyey-Greenstein asymmetry factor and is defined as [15],

$$g_\lambda = \frac{1}{4\pi} \int_{4\pi} \Phi_\lambda(\Theta) cos\Theta d\Omega \tag{6}$$

Under single scattering regime, the radiation characteristics of microorganisms are linearly dependent on concentration [14]. Thus, it is more convenient to introduce the mass extinction and absorption cross-sections, denoted by $E_{ext,\lambda}$ and $A_{abs,\lambda}$, respectively, and expressed in m^2/kg. They are defined as [14],

$$E_{ext,\lambda} = \frac{\beta_\lambda}{X} \quad \text{and} \quad A_{abs,\lambda} = \frac{\kappa_\lambda}{X} \tag{7}$$

where X is the concentration of the microorganisms, expressed in kg dry cell weight per m^3 of liquid medium. Similarly, the scattering coefficient σ_λ and the mass scattering cross-section $S_{sca,\lambda}$ expressed in m^2/kg are defined as,

$$\sigma_\lambda = \beta_\lambda - \kappa_\lambda \quad \text{and} \quad S_{sca,\lambda} = \frac{\sigma_\lambda}{X} \tag{8}$$

The extinction coefficient β_λ is obtained from normal-normal transmittance measurements of dilute suspensions [15]. The most common technique uses a spectrophotometer where a collimated monochromatic beam is incident on a cuvette containing the sample [15]. The transmitted light is focused onto a pinhole in front of the detector to eliminate the scattered light in directions other than the normal direction [25]. Bohren and Huffman [25] indicated that for reliable measurement of the extinction coefficient of highly forward scattering samples, the half acceptance angle of the detector Θ_a has to satisfy

$$\Theta_a < \frac{1}{2x} \tag{9}$$

where x_λ is the size parameter defined as [15],

$$x_\lambda = \frac{2\pi a n_\lambda}{\lambda} \tag{10}$$

Here, a is the scattering particle radius, n_λ is the refractive index of the non-absorbing and non-scattering medium in which the particles are submerged. Furthermore, to eliminate the effects of diffraction and multiple reflections from the container walls, the measurements are

taken with respect to a cuvette containing the above mentioned medium alone. In a different technique, Daniel and Incropera [26] measured the extinction coefficient of unicellular green algae *Chlorella pyrenoidosa* using a fiber-optic probe submerged in the microorganism suspension thus, eliminating possible reflection and refraction by the container walls. The probe had a half angle of view of 1.28 degree (in water) and the sample was illuminated by a collimated beam of diameter 71 mm (Xenon Arc Lamp).

Moreover, a large body of literature exists on measuring the absorption coefficient κ_λ both in the field (in situ) and in the laboratory. In situ measurements usually deal with extremely small concentration of microorganisms and are designed to overcome this difficulty by increasing the path length of the sample. Some of these methods include:

- *Reflecting tube absorption meter.* This technique uses a tube with reflective walls as the sample holder [27, 28]. The tube is illuminated with collimated monochromatic light at one end. As the light propagates through the sample it gets absorbed and scattered. The scattered light is reflected from walls and detected at the other end together with the transmitted light. The optical pathlength of the detected scattered light is larger than that of the transmitted light resulting in over estimation of the absorption coefficient.

- *Isotropic point source techniques.* This technique relies on the principle that irradiance from an isotropic point source decays proportional to $exp(-\kappa R)/R^2$, where R is the radial distance from the source [29]. Thus, the absorption coefficient can be obtained by measuring the irradiance at different radial distances from the source. This method is valid for under single scattering regime and enables the measurement of small absorption coefficients of natural waters.

Furthermore, some of the laboratory techniques for measuring the absorption coefficient include:

- *Integrating cavity absorption meter.* This technique uses a special sample holder known as the integrating cavity made of two concentric cavities separated by a diffuse translucent wall [30]. The sample is contained in the innermost cavity and is illuminated homogenously from all directions with monochromatic light delivered by a set of fiber-optics. The attenuated light is detected by two sets of fiber-optics at two different radial locations with respect to the sample. The device is calibrated with Irgalan Black and Alcian Blue solutions of known absorption characteristics taking into account the geometry of the device. This device is regarded as one of the most accurate methods for measuring the absorption coefficient [24].

- *Photoacoustic technique.* In this technique, the sample is irradiated with a beam of light chopped at some arbitrary frequency [15]. The absorbed light is dissipated as heat causing periodic changes in sample temperature. These temperature changes give rise to pressure oscillations which can be detected by a microphone and correlated to the absorption coefficient of the particles [31].

- *Integrating sphere technique.* This method relies on the fact that microorganism suspensions scatter light strongly in the forward direction [14, 22, 26]. Thus, a significant

portion of the forward scattered radiation is collected by the integrating sphere which has a large acceptance angle. Thus, the attenuation in the transmitted radiation is attributed solely to the effect of absorption. However, absorption coefficient obtained with this method suffers from scattering error [17, 32, 33]. Several correction methods have been suggested by Davies-Colley [17], Merzlyak and Naqvi [34], and Stramski and Piskozub [33]. The method reported by Davies-Colley [17] will be explained in detail in the next section.

Finally, the scattering phase function Φ_λ is measured using a nephelometer [25]. A typical nephelometer is comprised of a detector with a small acceptance angle that can measure the scattered radiation as a function of the polar and the azimuthal angles. A recent review of different nephelometer designs was given by Jonasz and Fournier [24]. For spherical or randomly oriented particles, as in the case of well mixed microorganism suspensions, the phase function does not change as a function of the azimuthal angle [15]. Thus, most nephelometers meassure Φ_λ as a function of the polar angle Θ only. Moreover, the scattering phase function for large particles does not vary significantly with wavelength at scattering angles less than 15^o [16]. Since most of the scattered light is in the forward direction, phase function measurements taken at 632.8 nm can be used as a first approximation for modeling light transfer in photobioreactors over the photosynthetically active region (PAR) ranging from 400 to 700 nm.

To the best of our knowledge, this work presents, for the first time, experimental measurements of the radiation characteristics of the hydrogen producing green algae *C.reinhardtii* CC125 and its truncated chlorophyll antenna transformants *tla1*, *tlaX*, and *tla1*-CW$^+$ over the spectral range from 300 to 1,300 nm as well as their scattering phase function at 632.8 nm.

3 MATERIALS AND METHODS

Microorganism Cultivation and Sample Preparation

C.reinhardtii is a unicellular green algae in the shape of a spheroid measuring about 10 μm in diameter. All strains were cultivated heterotrophically under aerobic conditions in TAP medium [35] with irradiance of 2,000 to 3,000 lux provided by fluorescent light bulbs (Ecologic by Sylvania, USA). The pH of the medium was 7.3. Samples were taken from actively growing cultures of each strain during their exponential growth phase. In order to eliminate the absorption and scattering due to the nutrient media, the microorganisms were centrifuged at 2,000 rpm for 5 minutes (Super T21 by Sorvall, USA), washed, and suspended in phosphate buffer saline (PBS) solution. While measuring their radiation characteristics, the microorganisms should not be suspended in distilled water [36]. Indeed, due to the large osmotic gradient between the inside of the cells and pure water, the cells will absorb water and stretch, with a concomitant change in their radiation characteristics. However, PBS solution overcomes this problem and provides a non-scattering medium, suitable for optical measurements [36]. One liter of PBS solution contains 8 g $NaCl$, 0.2 g KCl, 1.15 g $Na_2HPO_4 \cdot 7H_2O$, and 0.2 g KH_2PO_4. The refractive index of the PBS solution was measured with an abbe refractormeter (Leica USA, Model Mark II Plus) and found to be 1.3341 at 21^o C.

Figure 1 shows the in vivo differential interference contrast (DIC) and chlorophyll fluorescence micrographs of all strains. The images were obtained using Zeiss 510 confocal scanning laser microscope in the transmission and epi-fluorescence mode simultaneously as reported by Chen and Melis [37]. The excitation was provided by a Helium Neon laser at 543 nm while the chlorophyll fluorescence emission was detected in the red region with a long pass filter with a cut-off wavelength of 560 nm placed in front of the detector. It illustrates the size and shape of each strain as well as the location of the chlorophyll pigments which fluoresce in red [35]. The strong red fluorescence observed in the wild strain CC125 qualitatively shows that it has the largest concentration of chlorophyll while *tlaX* has the least. In addition, the cell size distribution has been quantified for each strain using a 100 μm deep hemacytometer (Hausser Scientific, USA, Model 1490) and the image processing and analysis software ImageJ [38]. The software approximates the cells as ellipses and reports the primary and secondary axes as major and minor diameters. For each strain, over 400 cells were counted. Figure 2 shows the number frequency of the major and minor diameters of the cells for all

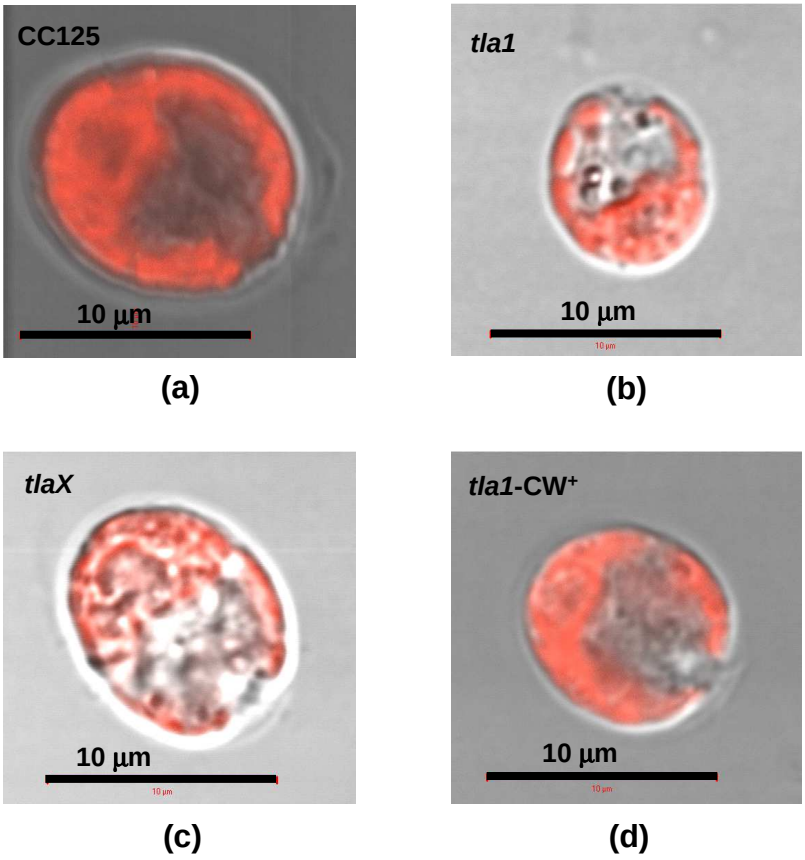

Figure 1: Differential interference contrast and fluorescence micrographs of (a)CC125, (b)*tla1*, (c)*tlaX*, and *tla1*-CW$^+$. The scale bars correspond to 10 μm.

strains with bins of width 0.1 μm. It indicates that *tla1* has the smallest mean major and minor diameters of 8.4 and 7.4 μm, respectively, while those of *tla1*-CW$^+$ were largest and equal to 10.3 and 8.9 μm. Moreover, *tlaX* had the largest standard deviation of 2.4 and 2.6

μm for the major and minor diameters, respectively. The mean major and minor diameters along with their standard deviations have been summarized in Table 1. In addition, Table 1 reports (i) the circularity defined as 4π(area of the cell/perimeter of the cell)^2 [38], and (ii) the Ferret diameters defined as the longest distance between two points along the perimeter of a particle [38], for all strains. Note that observations under the optical microscope establish that the size and shape of all strains investigated remain the same in PBS as in the nutrient media.

Table 1: Mean diameters, their standard deviations, circularity, and Ferret diameters of all strains.

	CC125	***tla1***	***tlaX***	***tla1*-CW$^+$**
Average major diameter (μm)	8.9	8.4	9.4	10.3
Standard deviation of major diameter (μm)	1.6	1.3	2.4	2.3
Average minor diameter (μm)	7.8	7.9	8.1	8.9
Standard deviation of minor diameter (μm)	1.6	1.3	2.6	2.2
Circularity	0.86	0.9	0.8	0.8
Ferret diameter (μm)	9.2	8.8	9.8	10.6

Three dilutions of each strain were prepared. Microorganism concentration of each dilution was determined using calibration curves that relate the optical density (OD) at 750 nm of a microorganism suspension to both the dry cell weight and the number of cells per unit volume of liquid [35]. The optical density is defined as $OD = -log_{10}(T_{750}/T_{750,PBS})$, where T_{750} and $T_{750,PBS}$ are the transmittance at 750 nm of the microorganism suspension in PBS and of PBS alone, respectively. The calibration curves were created by measuring the dry cell weight and the number of cells per unit volume at a given OD. First, the OD of the microorganisms was measured in disposable polystyrene cuvettes with light path of 10 mm at 750 nm [39] using a UV-Vis spectrophotometer (Cary-3E by Varian, USA). Then the cells were counted using the hemacytometer and ImageJ software. Finally, the microorganism suspensions were filtered through mixed cellulose filter membranes with 0.45 μm pore size (HAWP-04700 by Millipore, USA) and dried at 85^{o}C over night. The dried filters were weighed immediately after being taken out of the oven on a precision balance (model AT261 by Delta Range Factory, USA) with a precision of 0.01 mg. Figures 3(a) and (b) show the dry cell weight in kg dry cell/m^3 and the number density in number of cells/m^3, respectively, versus OD at 750 nm calibration curves for all strains using a 1 cm pathlength cuvette. It indicates that for all strains, 1 unit of OD at 750 nm corresponds to a microorganism concentration of 0.367 kg dry cell/m^3 and 2.79×10^6 cells/m^3.

Finally, the chlorophyll *a* and chlorophyll *b* concentrations were determined for each strain using the ethanol extraction method developed by Wintermans and De Mots [35]. Table 2 summarizes the chlorophyll *a*, chlorophyll *b*, and total chlorophyll concentrations for all strains in gram of chlorophyll per kilogram dry cell of microorganism. It indicates that all genetically engineered strains indeed contain both less chlorophyll *a* and *b* than the wild strain. Moreover, CC125, *tla1*, and *tla1*-CW$^+$ had half as much chlorophyll *b* than chlorophyll *a* whereas strain *tlaX* had about hundred times less chlorophyll *b* than chlorophyll *a*. Note that *tla1*-CW$^+$ has more chlorophyll *a* and *b* than *tla1*. This is most likely due to the fact that *tla1*-CW$^+$ was an offspring of *tla1* and the wild strain CC1068 [19]. Overall, these results corroborate with qualitative observations made in Figure 1.

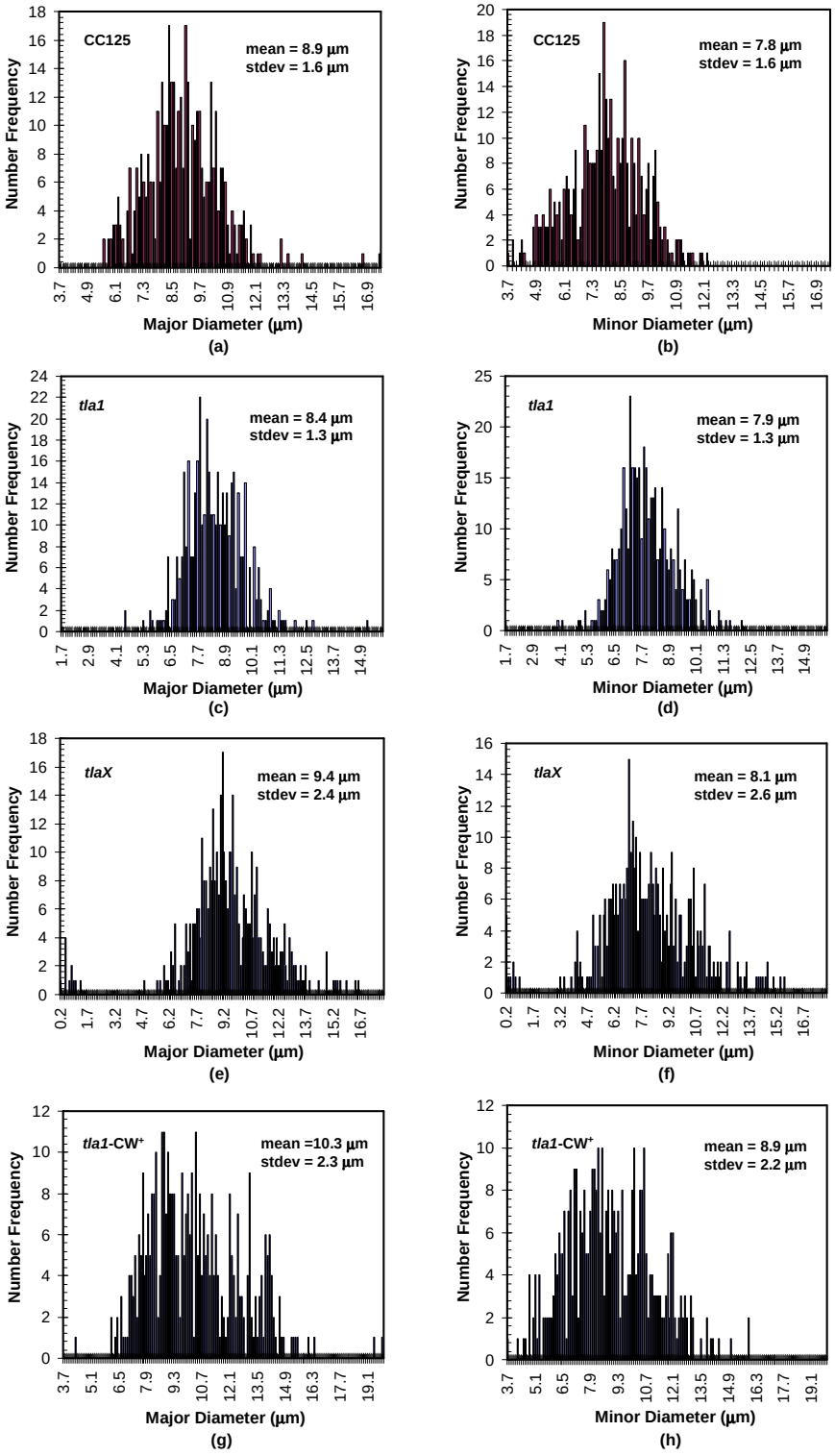

Figure 2: Number frequency of the major and minor cell diameters of (a,b) CC125, (c,d) *tla1*, (e,f) *tlaX*, and (g,h) *tla1*-CW$^+$.

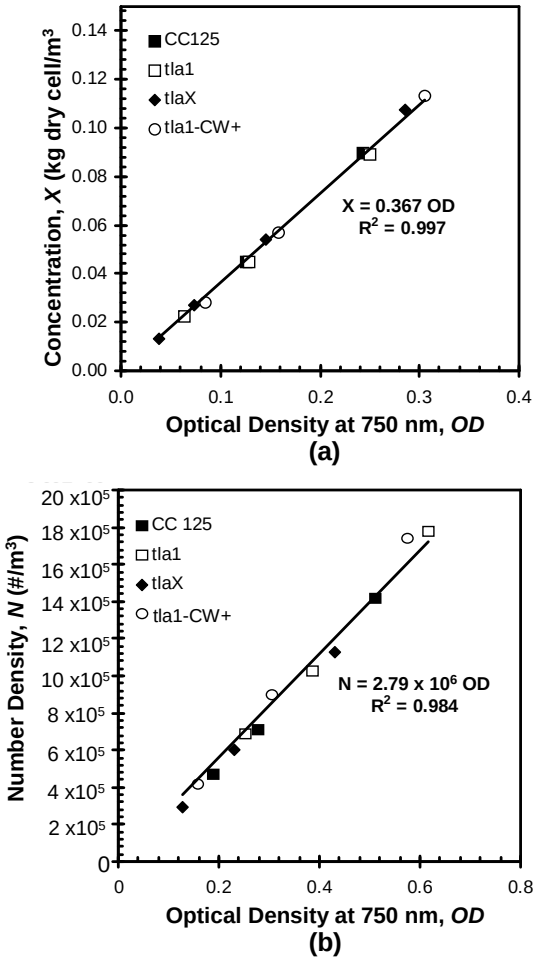

Figure 3: Calibration curves of (a) dry cell weight and (b) number density versus optical density (OD) at 750 nm for all strains.

Table 2: Chlorophyll (Chl) concentrations of all *C.reinhardtii* strains determined by ethanol extraction [35].

Strain	**Chl *a* (g/kg dry cell)**	**Chl *b* (g/kg dry cell)**	**Total Chl (g/kg dry cell)**
CC125	29.80 ± 2.03	14.53 ± 1.11	44.33 ± 3.14
tla1	18.98 ± 1.36	8.67 ± 0.66	27.65 ± 2.02
tlaX	16.82 ± 0.24	0.16 ± 0.07	16.98 ± 0.31
37RP-tla1	22.24 ± 2.17	10.34 ± 0.98	32.57 ± 3.15

Experimental Procedure and Analysis

In measuring the radiation characteristics, the following assumptions are made: (1) the microorganisms are well mixed and randomly oriented, (2) for all measurements, the pathlength and the concentration of the samples is such that single scattering prevails, i.e., photons undergo one scattering event at most as they travel through the suspension, (3) the scattering phase function has azimuthal symmetry and is only a function of the polar angle, and (4)

the scattering phase function is independent of wavelength in the spectral range of interest from 300 to 1,300 nm.

First, a polar nephelometer has been constructed to experimentally measure the scattering phase function of microorganisms at 632.8 nm. The details of the experimental setup and its validation have been reported elsewhere [40] and need not be repeated. The nephelometer featured a fiber optic probe with a miniature Gershun tube that limits the half acceptance angle of the detector to 0.7^o in water. The nephelometer measured the scattered intensity I_λ in $\mathrm{Wm^{-2}sr^{-1}}$ as a function of the polar angle Θ. The scattering phase function was recovered using the analysis suggested by Privoznik *et al.* [26],

$$\Phi_\lambda(\Theta) = \frac{2I_\lambda(\Theta)[U_\lambda(\Theta)]^{-1}}{\int_0^\pi I_\lambda(\Theta)[U_\lambda(\Theta)]^{-1} sin\Theta d\Theta} \tag{11}$$

The geometrical correction term $U_\lambda(\Theta)$ accounts for the variation of the scattering volume and the pathlength between the scattering volume center and the detector with detection angle and is given by [22],

$$\begin{aligned} U_\lambda(\Theta) \quad = & \int_0^{w/sin\Theta} \left[1 + \beta_\lambda \frac{w}{2} ctan\Theta - \beta_\lambda L cos\Theta\right] \\ & \left[1 - \beta_\lambda \left(r - \frac{w}{2sin\Theta}\right)\right] \left[1 - \beta_\lambda \left(\frac{w}{sin\Theta} - L\right)\right] dL \end{aligned} \tag{12}$$

where w is the beam diameter equal to 1.7×10^{-3} m, r is the radius of rotation of the fiber-optic probe, equal to 6×10^{-3} m, and L is the coordinate direction along the line of sight of the detector, marking the length of the scattering volume as shown in Figure 4. The pathlength of the radiation reaching the detector is denoted by $P = w/2sin\Theta + r$ [22]. Note that due to the finite size of the probe and the beam, data could only be obtained for scattering angle Θ up to to 160^o where the probe did not obstruct the incident beam.

The extinction coefficient $\beta_{632.8}$ was measured with the nephelometer at wavelength 632.8 nm. In this method, the radiation flux $F_\lambda(z)$, expressed in $\mathrm{Wm^{-2}}$, at two different locations z_1 and z_2 along the path of a divergent incident beam are measured. The extinction coefficient was evaluated as [22],

$$\beta_{632.8} = \frac{ln\left|F_{632.8}(z_2)/F_{632.8}(z_1)\right| + ln\left|z_1^2/z_2^2\right|}{z_1 - z_2} \tag{13}$$

where z is the distance between the detector and the virtual image of the last lens in the optical setup shown in Figure 4. Note that the second term in the numerator accounts for the divergence of the incident beam. At all angles, the experimental value of $\beta_{632.8}P$ was less than 0.1 ensuring single scattering [22].

Then, the extinction coefficients β_λ of the four strains of *C.reinhardtii* were measured from normal-normal transmittance measurements $T_{\lambda,X}$ over the spectral range from 300 to 1,300 nm using a UV-VIS-NIR spectrophotometer (Shimadzu, USA, Model UV-3101PC). All

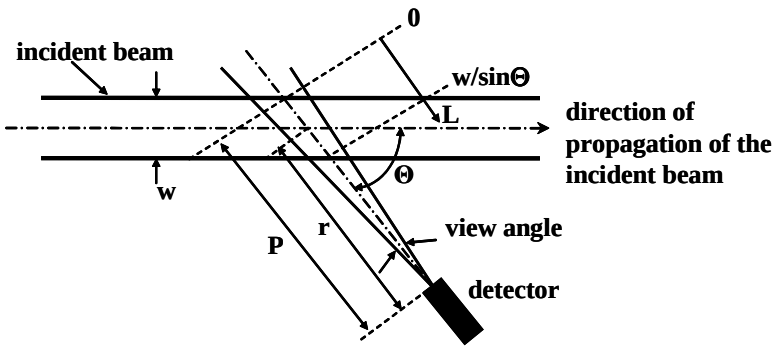

Figure 4: Coordinate system used in recovering the scattering phase function from the measured intensity distribution [26].

the transmission measurements were carried out in a liquid flow cell of pathlength t equal to 0.001 m with quartz windows (FT04-060 by Thermo, USA). During the measurements, the microorganism suspension was continuously flown through the flow cell with a peristaltic pump (4049 K33 by McMaster, USA) at a flow rate of approximately 10 mL/min to avoid settling of microorganisms. In order to account for reflection and refraction by the flow cell, measurements were made with respect to the transmission spectrum of PBS alone denoted by $T_{\lambda,PBS}$.

Due to its large acceptance angle of about 3^o, the spectrophotometer measured an apparent extinction coefficient χ_λ given as [17, 32],

$$\chi_\lambda = -\frac{1}{t} ln \left(\frac{T_{\lambda,X}}{T_{\lambda,PBS}} \right) \tag{14}$$

The apparent extinction coefficient is related to the absorption and extinction coefficients through [17, 32],

$$\chi_\lambda = \kappa_\lambda + \sigma_\lambda - \epsilon_n \sigma_\lambda \tag{15}$$

where ϵ_n represents the portion of the light scattered in the forward direction and detected by the spectrophotometer in directions other than the the normal direction due to the finite size of the acceptance angle. It is defined as [41, 42],

$$\epsilon_n = \frac{1}{2} \int_0^{\Theta_a} \Phi_\lambda(\Theta) sin\Theta d\Theta \tag{16}$$

where Θ_a is the half acceptance angle of the detector. Using Equation (15), the extinction coefficient can be determined as,

$$\beta_\lambda = \frac{\chi_\lambda - \epsilon_n \kappa_\lambda}{1 - \epsilon_n} \tag{17}$$

Finally, the absorption coefficient κ_λ was determined from the hemispherical transmittance measurements performed with an integrating sphere [22]. The measurements were corrected for scattering errors using the analysis suggested by Davies-Colley [17]. Under single scattering conditions, the apparent absorption coefficient $\chi_{h,\lambda}$ is related to the hemispherical

transmittance of the microorganism sample $T_{h,\lambda,X}$ by [17],

$$\chi_{h,\lambda} = -\frac{1}{t} ln \left(\frac{T_{h,\lambda,X}}{T_{h,\lambda,PBS}} \right) \tag{18}$$

where $T_{h,\lambda,PBS}$ is the normal-hemispherical transmittance of the PBS solution alone. Due to the geometry of the experimental setup all the scattered radiation cannot be captured and measured by the integrating sphere. Thus, $\chi_{h,\lambda}$ overestimates the actual absorption coefficient which can be retrieved as [17],

$$\kappa_\lambda = \chi_{h,\lambda} - (1 - \epsilon_h)\sigma_\lambda \tag{19}$$

where ϵ_h is the fraction of scattered light detected by the integrating sphere. Ideally, ϵ_h is equal to unity when all light scattered in all directions is collected and detected by the integrating sphere. In order to account for the scattering error, Davies-Colley [17] assumed that the microorganisms do not absorb radiation at wavelength λ_o, in this case λ_o=750 nm for *A.variabilis* and λ_o=900 nm for *R.sphaeroides*. At this wavelength, the apparent absorption coefficient is equal to the scattering error given as,

$$\chi_{h,\lambda_o} = (1 - \epsilon_h)\sigma_{\lambda_o} \tag{20}$$

Combining Equations (19) and (20) yields,

$$\kappa_\lambda = \chi_{h,\lambda} - \chi_{h,\lambda_o} \frac{\sigma_\lambda}{\sigma_{\lambda_o}} \qquad \text{where} \qquad \frac{\sigma_\lambda}{\sigma_{750}} = \frac{\chi_\lambda - \chi_{h,\lambda}}{\chi_{750} - \chi_{h,750}} \tag{21}$$

Validations

First, measurements using the nephelometer and the procedure to analyze the data have been successfully validated with polystyrene spheres of 19 μm in diameter and with glass fibers of 10 mm in length and 17 μm in diameter [40].

The experimental setup and analysis for measuring the extinction, absorption, and scattering coefficients have also been successfully validated against predictions from Mie theory using polystyrene microspheres with diameter of 5 μm and standard deviation of 0.6 μm supplied by Duke Scientific Corp., USA (Part No: 2005A). Figure 5 compares the extinction, absorption, and scattering cross-sections of the microspheres predicted by Mie theory with the uncorrected experimental results [using Equations (14) and (18)] and the corrected results [using Equations (17) and (21)] over the spectral range from 400 to 800 nm. It shows that predictions from Mie theory lie within the experimental uncertainty of the corrected experimental data estimated to be 14% for both the extinction and scattering cross-sections and within 6% for the absorption cross-section. The experimental uncertainties in cross-sections were estimated from the propagation of uncertainties in measuring the normal-normal and normal-hemispherical transmittances, the factors ϵ_n and ϵ_h, and the concentration of the polystyrene microspheres. Note that in our Mie theory calculations, the spheres were assumed to be non-absorbing, i.e., their absorption cross-section was equal to zero over the entire spectral range of interest.

In summary, the experimental apparatus and data analysis procedure were successfully validated. It has been established that correcting for the forward scattering is necessary for accurately measuring both the extinction and the absorption coefficients. The experimental results reported from hereon correspond to the corrected data.

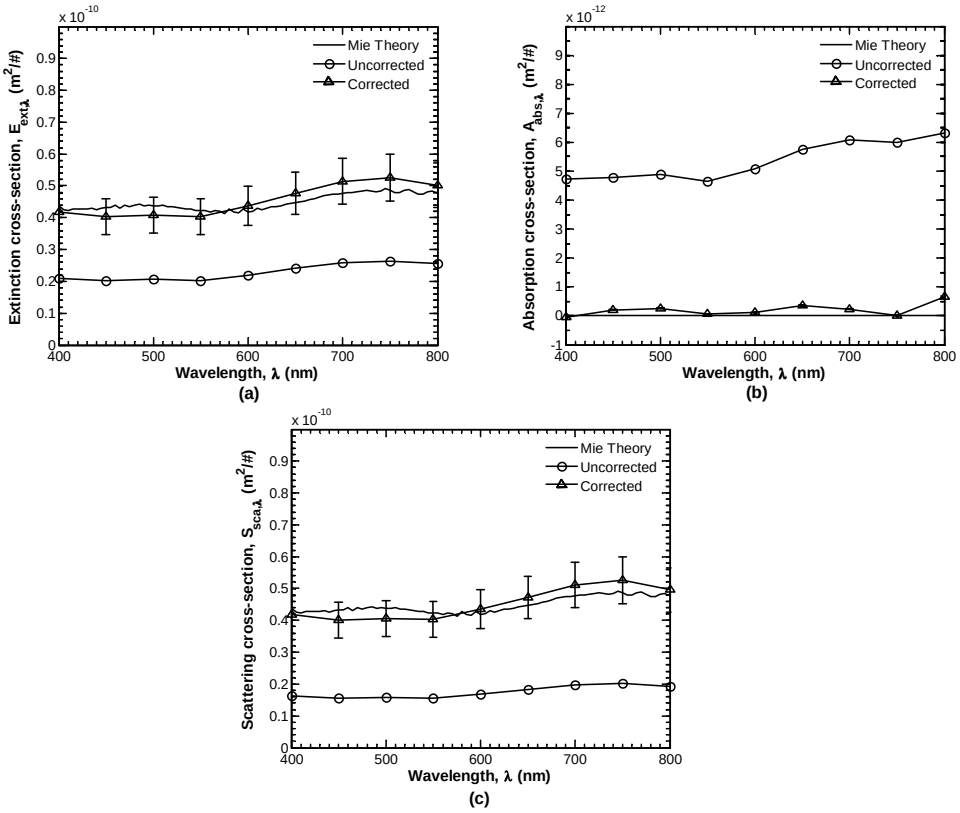

Figure 5: Comparison of the experimentally measured uncorrected and corrected (a) extinction, (b) absorption, and (c) scattering cross-sections of 5 μm diameter polystyrene microspheres with those predicted by the Mie theory.

4 RESULTS AND DISCUSSION

All transmittance measurements were performed twice and the arithmetic average of the results is reported. The relative difference between the replica measurements was less than 0.1% over the entire spectral region considered and for all microorganisms.

Cross-sections of the Wild Strain

Figures 6(a), (c), and (e) show the absorption κ_λ, scattering σ_λ, and extinction β_λ coefficients of *C.reinhardtii* CC125, respectively, measured at three different microorganism concentrations, namely 0.0898, 0.1386, and 0.1840 kg/m^3 in the spectral region from 300 to 1,300 nm. Figure 6(a) shows that *C.reinhardtii* CC125 have absorption peaks at 435, 475, and 676 nm. The peaks at 435 nm and 676 nm correspond to the absorption peaks of in vivo chlorophyll *a*. In addition in vivo chlorophyll *b* has absorption peaks at 475 nm and at 650 nm. Thus, the absorption peak at 475 nm and the peak broadening around 650 nm observed in Figure 6(a) can be attributed to the presence of chlorophyll *b*. The chlorophyll *a* and *b* pigments are responsible for absorbing solar radiation and generating electrons that drive the metabolic reactions of the microorganisms.

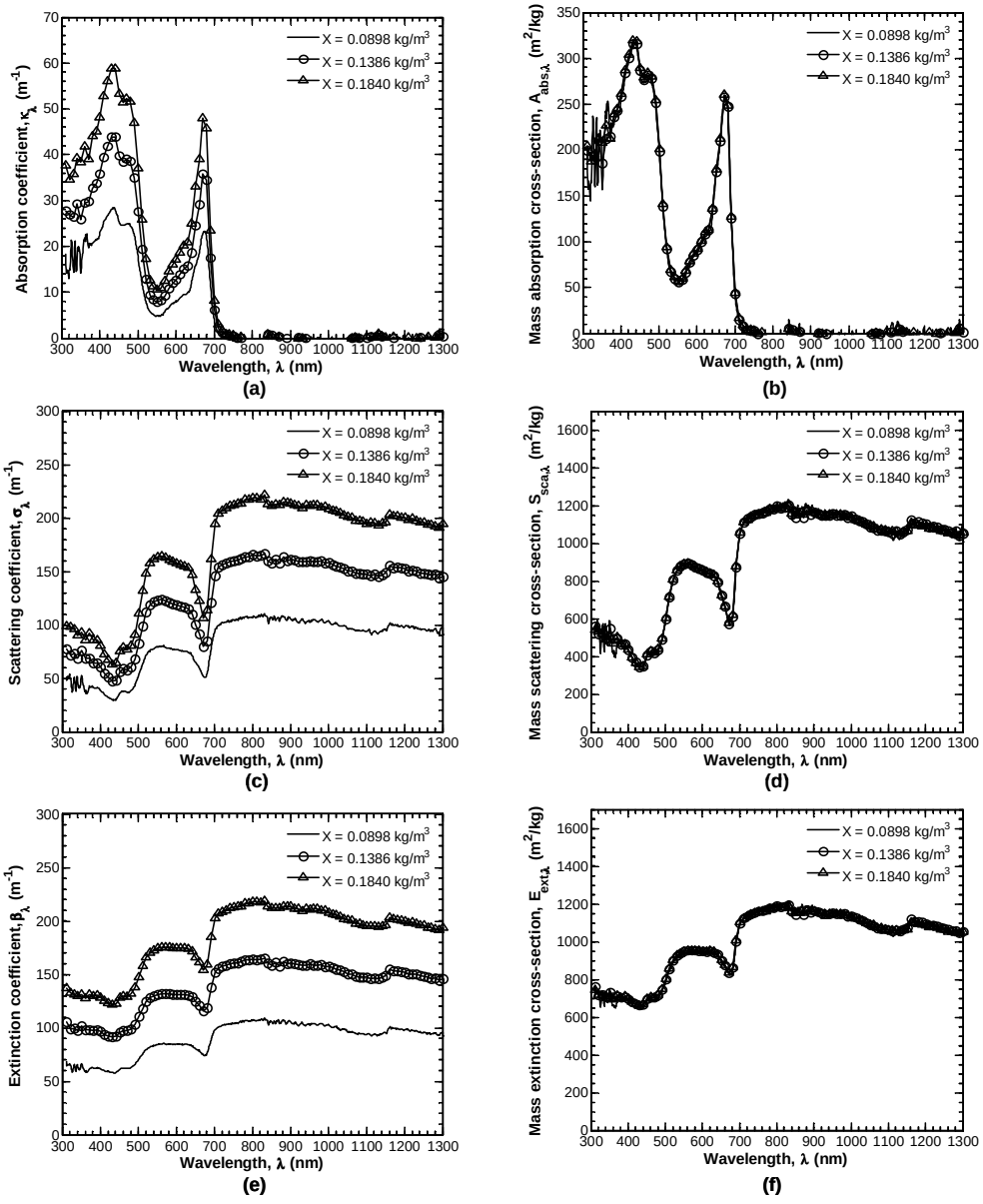

Figure 6: The (a) absorption κ_λ, (c) scattering σ_λ, and (d) extinction β_λ coefficients and the corresponding (b) mass absorption $A_{abs,\lambda}$, (d) mass scattering $S_{sca,\lambda}$, and (f) mass extinction $E_{ext,\lambda}$ cross-sections of *C.reinhardtii* CC125 over the spectral range from 300 to 1,300 nm at three different microorganism concentrations.

In addition, Figures 6(b), (d), and (f) show the spectral mass absorption, mass scattering, and mass extinction cross-sections $A_{abs,\lambda}$, $S_{sca,\lambda}$, and $E_{ext,\lambda}$ over the spectral region from 300 to 1,300 nm. It establishes that $A_{abs,\lambda}$, $S_{sca,\lambda}$, and $E_{ext,\lambda}$ are independent of concentration X as they collapse on a single line for different microorganism concentrations. This also shows that multiple scattering is negligible for the concentrations considered as assumed in the data analysis.

Cross-sections of the Transformants

The coefficients κ_λ, σ_λ, and β_λ and the cross-sections $A_{abs,\lambda}$, $S_{sca,\lambda}$, and $E_{ext,\lambda}$ of the strains *tla1*, *tlaX*, and *tla1*-CW$^+$ were obtained in a similar manner and are presented in Figures 7 to 9, respectively. The general trends observed and the absorption peaks for the genetically engineered strains are similar to those found for the wild strain.

Comparisons Between the Wild Strain and the Transformants

In order to better appreciate the effect of genetic engineering on the radiation characteristics of the truncated chlorophyll antenna transformants, Figures 10(a) through (c) show the ratio of cross-sections $A_{abs,\lambda}$, $S_{sca,\lambda}$, and $E_{ext,\lambda}$ of *tla1*, *tla1*-CW$^+$, and *tlaX* to those of CC125, respectively. Figure 10(a) indicates that genetic engineering of *C.reinhardtii* CC125 reduces the absorption cross-section $A_{abs,\lambda}$ (i) by 25% to 45% for *tla1*, (ii) by 30% to 70% for *tlaX*, and (iii) by 5% to 15% for *tla1*-CW$^+$ over the spectral region from 400 to 700 nm, i.e., PAR. Note that the ratio of cross-sections with respect to those of the wild strain outside PAR gives very large and noisy results due to division by zero or very small numbers. Furthermore, these trends agree well with the measured chlorophyll concentrations of the strains summarized in Table 2. Moreover, for all wavelengths between 400 and 700 nm, *tlaX* absorbs less than *tla1* as expected a priori. This is especially apparent around the absorption peaks of chlorophyll *b* at 475 and 650 nm.

On the other hand, changes in the mass scattering cross-sections show an opposite trend to those observed for the mass absorption cross-sections. Figure 10(b) shows that the scattering cross-sections of *tla1*, *tlaX*, and *tla1*-CW$^+$ increase by up to 45%, 80%, and 25% respectively. The maximum increase is observed around the absorption peaks of *C.reinhardtii* CC125 around 435, 475, and 676 nm. Thus, as absorption is reduced, scattering becomes more important for the genetically engineered *C.reinhardtii*. Similar observations have been reported in the ocean optics literature where decrease in the absorption cross-section is compensated by an increase in the scattering cross-section [32]. Moreover, while CC125, *tlaX*, and *tla1*-CW$^+$ display similar scattering cross-sections in the spectral region from 700 to 1,300 nm, *tla1* feature a smaller scattering cross-section which decreases with increasing wavelength. This can be attributed to the fact that *tla1* lack cell walls the other strains have.

Moreover, Figure 10(c) illustrates the ratio of the extinction cross-section $E_{ext,\lambda}$ of *tla1*, *tlaX*, and *tla1*-CW$^+$ with respect to that of CC125. It shows that $E_{ext,\lambda}$ for *tla1* and *tla1*-CW$^+$ do not differ by more than 10% from that of CC125 in the spectral region from 300 to 700 nm. On the other hand, the extinction cross-section of *tlaX* increases as much as 25%. Furthermore, the extinction cross-sections of the strains with cell walls are identical in

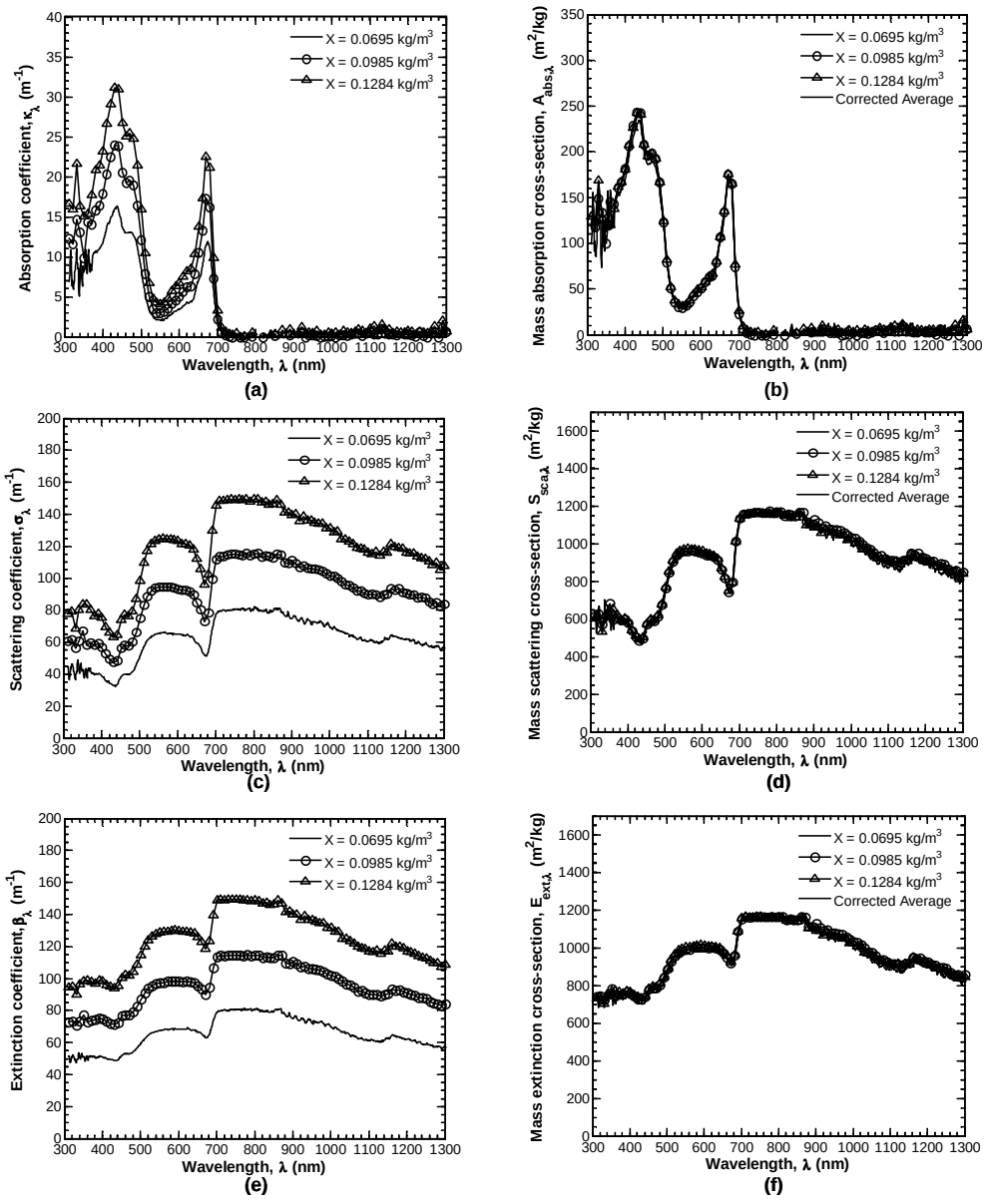

Figure 7: The (a) absorption κ_λ, (c) scattering σ_λ, and (d) extinction β_λ coefficients and the corresponding (b) mass absorption $A_{abs,\lambda}$, (d) mass scattering $S_{sca,\lambda}$, and (f) mass extinction $E_{ext,\lambda}$ cross-sections of *C.reinhardtii tla1* over the spectral range from 300 to 1,300 nm at three different microorganism concentrations.

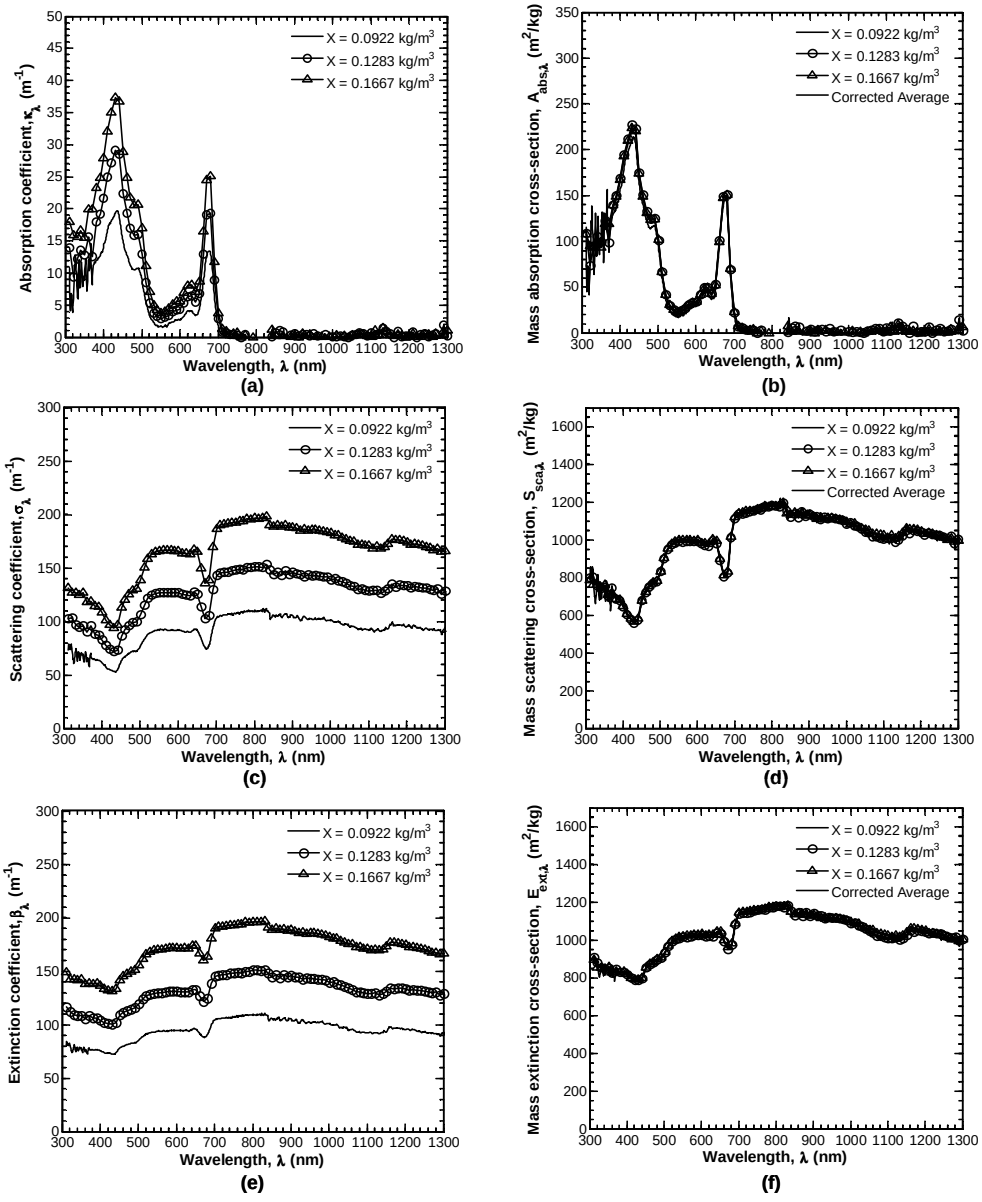

Figure 8: The (a) absorption κ_λ, (c) scattering σ_λ, and (d) extinction β_λ coefficients and the corresponding (b) mass absorption $A_{abs,\lambda}$, (d) mass scattering $S_{sca,\lambda}$, and (f) mass extinction $E_{ext,\lambda}$ cross-sections of *C.reinhardtii tlaX* over the spectral range from 300 to 1,300 nm at three different microorganism concentrations.

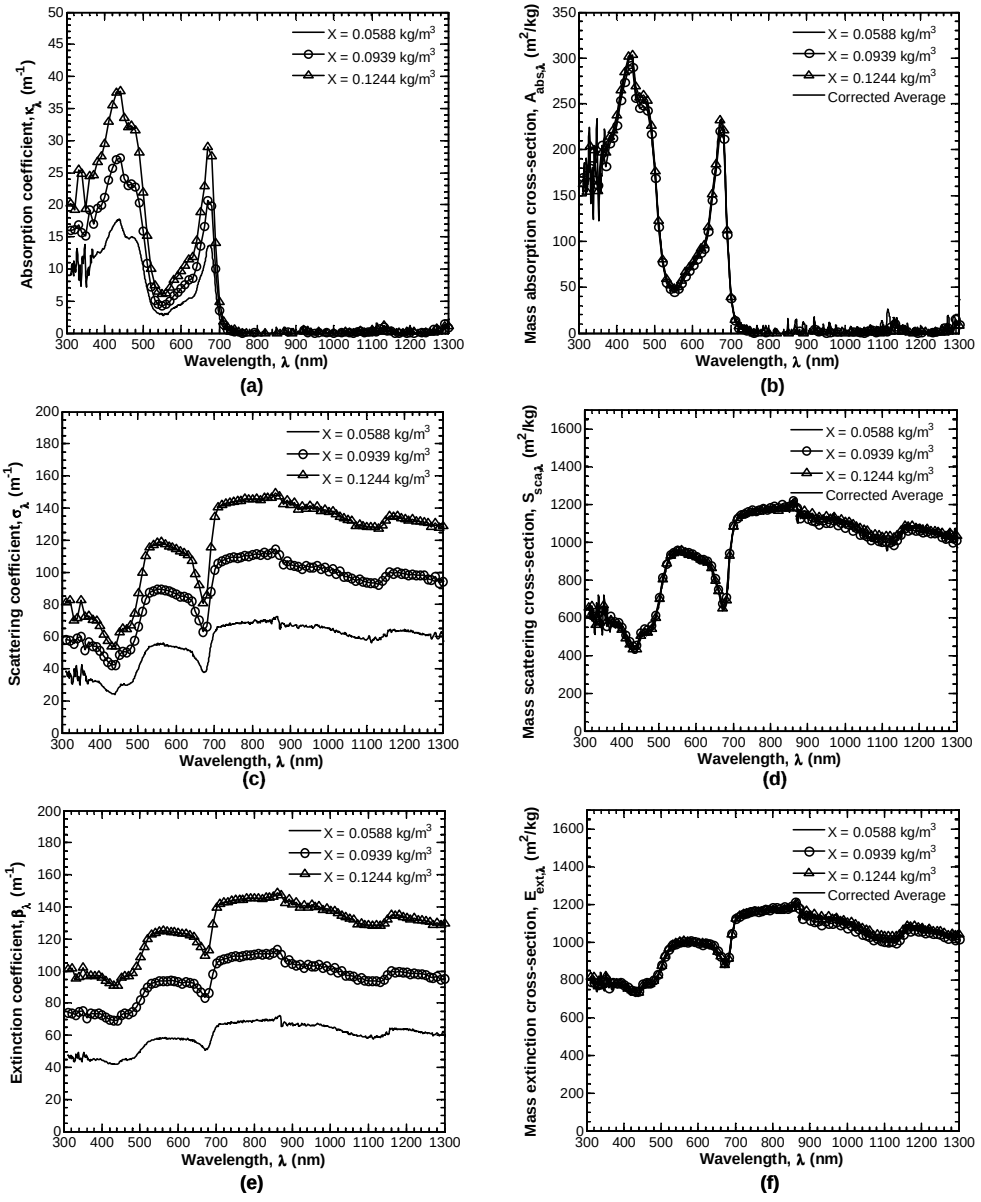

Figure 9: The (a) absorption κ_λ, (c) scattering σ_λ, and (d) extinction β_λ coefficients and the corresponding (b) mass absorption $A_{abs,\lambda}$, (d) mass scattering $S_{sca,\lambda}$, and (f) mass extinction $E_{ext,\lambda}$ cross-sections of *C.reinhardtii tla1*-CW$^+$ over the spectral range from 300 to 1,300 nm at three different microorganism concentrations.

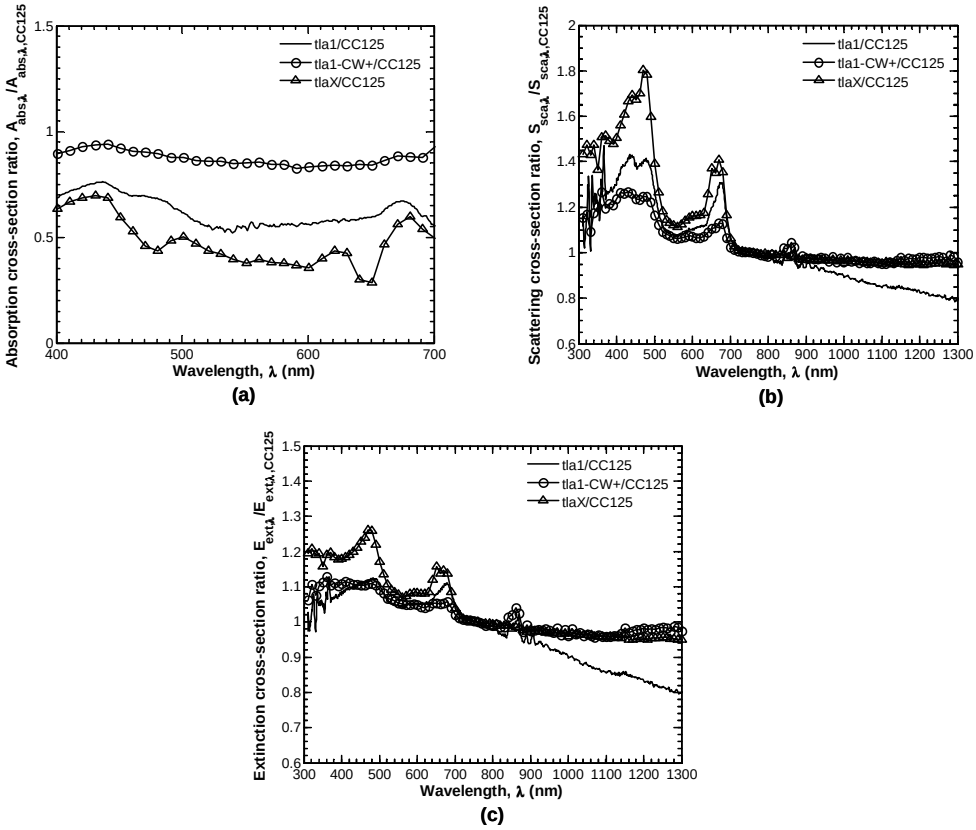

Figure 10: The ratio of the (a) mass absorption $A_{abs,\lambda}$ (b) mass scattering $S_{sca,\lambda}$, (c) mass extinction cross-sections $E_{ext,\lambda}$ of *tla1*, *tla1*-CW$^+$, and *tlaX* with respect to those of *C.reinhardtii* CC125 over the spectral range from 300 to 1,300 nm.

the spectral region from 700 to 1,300 nm. However, similar to the scattering cross-sections, the extinction cross-section of *tla1* decreases with increasing wavelength with respect to those of the strains with cell walls. Although chlorophyll antenna reduction does not reduce the extinction cross-sections of the mutants, it has several advantages enabling improved photosynthetic efficiency. First of all, reduction in chlorophyll antenna size increases the saturation irradiance of photosynthesis [9]. Thus, microorganisms can conduct photosynthesis at larger irrandiances without incurring photooxidative damage. Note that the results of Polle *et al.* [19] were conducted at very large irradiance of 1,500 μmol/m^2/s. Moreover, reducing the chlorophyll antenna size increases the quantum efficiency of photosynthesis at large irradiances [8]. This is because, photons are not absorbed and wasted as heat and fluorescence by a given microorganism but scattered, mainly in the forward direction, increasing their chance of being used by other microorganisms. Finally, since scattering is mainly in the forward direction, the effect of increase in scattering cross-section on the local irradiance within the photobioreactor is not trivial and requires detailed radiation transfer analysis. However, this analysis falls beyond the scope of the present study.

The single scattering albedo ω_λ represents the contribution of scattering to the overall extinction and is shown in Figure 11(a) for all strains. The figure establishes that the

single scattering albedo for all strains is greater than 0.5 and scattering dominates over absorption over the entire spectrum. Then, accurate knowledge of the scattering phase function $\Phi_\lambda(\Theta)$ of the microorganisms and solution of the RTE are required for accurate simulation, modeling, and optimization of the photobioreactor as established by Berberoğlu *et al.* [14]. In particular, the commonly used Beer-Lambert's law is no longer valid as it does not distinguish between absorption and scattering phenomena and ignores in-scattering (path radiance) represented by the second term on the right-hand side of Equation (1) [14]. Furthermore, to better illustrate the effect of genetic engineering on ω_λ Figure 11(b) shows the ratio of the single scattering albedo of all strains with respect to that of the wild strain CC125. It indicates that ω_λ is larger than that of CC125 by up to 30%, 45%, and 15% for *tla1*, *tlaX*, and *tla1*-CW$^+$, respectively.

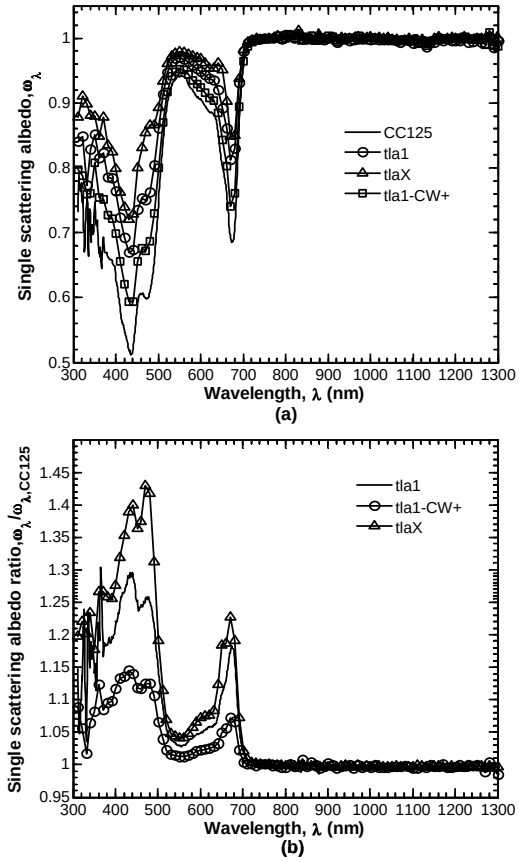

Figure 11: (a) The single scattering albedo ω_λ for all strains and (b) the ratio of the single scattering albedo of *tla1*, *tlaX*, and *tla1*-CW$^+$ with respect to that of *C.reinhardtii* CC125 over the spectral range from 300 to 1,300 nm.

Scattering Phase Functions of All Strains

Finally, the scattering phase functions of all strains are measured using the nephelometer at microorganism concentrations of 0.007 ± 0.002 kg/m^3 and at the wavelength of 632.8 nm.

Figure 12 shows the scattering phase functions of CC125, *tla1*, *tlaX*, and *tla1*-CW$^+$ measured by the nephelometer along with the truncated phase function (TPF) approximations. In TPF, the phase function is divided in two parts, from 0 to Θ_{cutoff} and from Θ_{cutoff} to π. Each part is a linear combination of two Henyey-Greenstein phase functions. The latter is given as [15],

$$\Phi_{HG} = \frac{1-g^2}{[1+g^2-2gcos\Theta]^{3/2}} \tag{22}$$

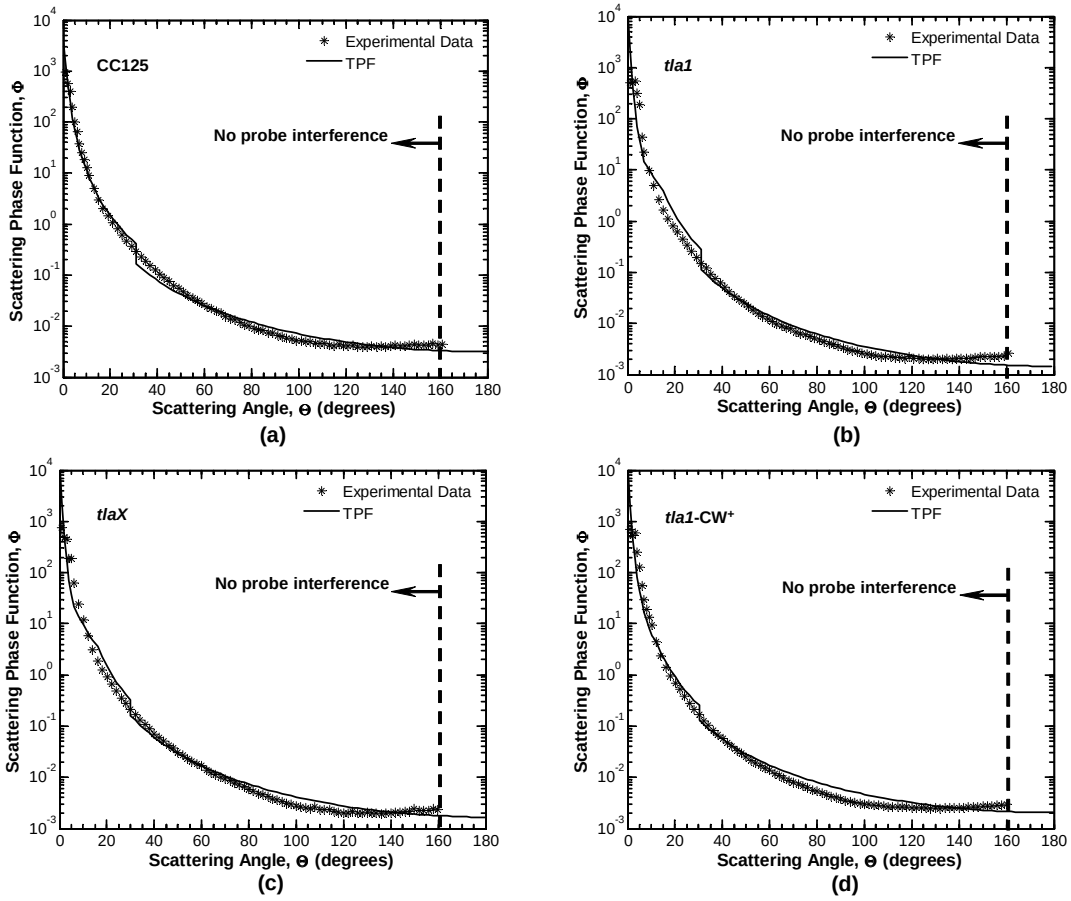

Figure 12: The scattering phase function of (a) CC125, (b) *tla1*, (c) *tlaX*, and (d) *tla1*-CW$^+$ at 632.8 nm obtained experimentally and the corresponding TPF approximation.

where g is the mean cosine of the scattering phase function, also known as the Henyey-Greenstein asymmetry factor. The TPF for the different strains is expressed as [14],

$$\begin{aligned} \Phi(\Theta) &= f_1\Phi_{HG,g_{TPF,1}}(\Theta) + (1-f_1)\Phi_{HG,g_{TPF,2}} \qquad \text{for} \quad 0 \le \Theta \le \Theta_{\text{cutoff}} \\ \Phi(\Theta) &= h_1\left[f_1\Phi_{HG,g_{TPF,1}}(\Theta) + (1-f_1)\Phi_{HG,g_{TPF,2}}\right] \qquad \text{for} \quad \Theta_{\text{cutoff}} < \Theta < \pi \end{aligned} \tag{23}$$

where f_1 and h_1 are weighing parameters and $g_{TPF,1}$, and $g_{TPF,2}$ are the asymmetry factors. These are determined by minimizing the sum of the squares of the error between experimentally obtained phase function and the TPF model. Note that the TPF function needs to be

normalized by the method previously adopted by Nicolau *et al.* [43]. The TPF parameters along with the Henyey-Greenstein asymmetry factors for all strains are summarized in Table 3. Figure 12 indicates that the scattering is mainly in the forward direction for all strains. Moreover, the scattering phase functions of all strains show similar trends. Finally, the TPF parameters indicate that the scattering phase function of the genetically engineered strains is peaked slightly more forward than the wild strain.

Table 3: Parameters associated with the TPF and Henyey-Greenstein approximations for the scattering phase function of all strains.

	CC125	***tla1***	***tlaX***	***tla1-CW*$^+$**
$g_{TPF,1}$	0.98	0.99	0.99	0.99
$g_{TPF,2}$	0.95	0.96	0.98	0.97
f_1	0.65	0.86	0.72	0.71
h_1	0.42	0.40	0.50	0.52
Θ_{cutoff}	30^o	30^o	30^o	30^o
g	0.98	0.99	0.99	0.98

5 CONCLUSION

This paper presents for the first time the radiation characteristics of *C.reinhardtii* CC125 and its truncated chlorophyll antenna transformants *tla1*, *tlaX*, and *tla1*-CW$^+$ over the spectral range from 300 to 1,300 nm as well as their scattering phase functions at 632.8 nm. It establishes that *C.reinhardtii* CC125 has major absorption peaks at 435 and 676 nm, corresponding to the in vivo absorption peaks of chlorophyll *a*, and at 475 nm corresponding to that of chlorophyll *b*. The genetically engineered strains have less chlorophyll pigments than the wild strain and thus have smaller absorption cross-sections. In particular, *tlaX* has the smallest absorption cross-section and the lowest chlorophyll *b* concentration of all strains. However, the reduction in the absorption cross-section is compensated by an increase in scattering cross-section of the genetically engineered strains.

Moreover, the single scattering albedo ω_λ is greater than 0.5 over the spectral region from 300 to 1,300 nm, indicating that scattering is the dominant phenomena contributing to the overall extinction. Although scattering dominates over absorption, it is mainly in the forward direction and reduction of absorption cross-section can still improve the performance of photobioreactors by increasing the saturation irradiance of algae and quantum efficiency of photobiological hydrogen production. Thus, optimizing light transport in the photobioreactor requires careful radiation transfer analysis [14]. The reported radiation characteristics should enable such accurate radiation transfer modeling of photobioreactors for hydrogen production. Finally, the experimental and analysis methods presented here can be used to accurately measure the radiation characteristics of other microorganisms for photobioreactors or ocean optics applications. Future work should evaluate the specific hydrogen production rate and light to hydrogen energy conversion efficiency of the genetically engineered microorganisms to ensure that pigment reduction has not adversely affected their hydrogen production metabolism.

ACKNOWLEDGEMENTS

The authors gratefully acknowledge the DOE HFC&IT Program for the generation of *tla1*, *tlaX*, and *tla1*-CW$^+$ as well as the support of the California Energy Commission through the Energy Innovation Small Grant (EISG 53723A/03-29; Project Manager: Michelle McGraw).

References

[1] O. Pulz, "Photobioreactors: production systems for phototrophic microorganisms", *Applied Microbiology and Biotechnology*, vol. 57, no. 3, pp. 287–293, 2001.

[2] N.J. Kim, I.S. Suh, B.K. Hur, and C.G. Lee, "Simple monodimensional model for linear growth rate of photosynthetic microorganisms in flat-plate photobioreactors", *Journal of Microbiology and Biotechnology*, vol. 12, pp. 962–971, 2002.

[3] S.A. Markov, R. Lichtl, K.K. Rao, and D.O. Hall, "A hollow fibre photobioreactor for continuous production of hydrogen by immobilized cyanobacteria under partial vacuum", *International Journal of Hydrogen Energy*, vol. 18, pp. 901–906, 1993.

[4] S.A. Markov, M.J. Bazin, and D.O. Hall, "Hydrogen photoproduction and carbon dioxide uptake by immobilized *Anabaena variabilis* in a hollow-fiber photobioreactor", *Enzyme Microbial Technology*, vol. 17, pp. 306–310, 1995.

[5] S.A. Markov, A.D. Thomas, M.J. Bazin, and D.O. Hall, "Photoproduction of hydrogen by cyanobacteria under partial vacuum in batch culture or in a photobioreactor", *International Journal of Hydrogen Energy*, vol. 22, pp. 521–524, 1997.

[6] A.A. Tsygankov, A.S. Fedorov, S.N. Kosourov, and K.K. Rao, "Hydrogen production by cyanobacteria in an automated outdoor photobioreactor under aerobic conditions", *Biotechnology and Bioengineering*, vol. 80, pp. 777–715, 2002.

[7] J.H. Yoon, J.H. Shin, M.S. Kim, S.J. Sim, and T.H. Park, "Evaluation of conversion efficiency of light to hydrogen energy by *Anabaena variabilis*", *International Journal of Hydrogen Energy*, vol. 31, pp. 721–727, 2006.

[8] A. Melis, "Green alga hydrogen production: process, challenges and prospects", *International Journal of Hydrogen Energy*, vol. 27, pp. 1217–1228, 2002.

[9] A. Melis, J. Neidhardt, and J.R. Benemann, "*Dunaliella salina (Chlorophyta)* with small chlorophyll antenna sizes exhibit higher photosynthetic productivities and photon use efficiencies than normally pigmented cells", *Journal of Applied Phycology*, vol. 10, pp. 515–525, 1999.

[10] J.F. Cornet, C.G. Dussap, and G. Dubertret, "A structured model for simulation of cultures of the cyanobacterium *Spirulina platensis* in photobioreactors: I. Coupling between light transfer and growth kinetics", *Biotechnology and Bioengineering*, vol. 40, pp. 817–825, 1992.

[11] J.F. Cornet, C.G. Dussap, P. Cluzel, and G. Dubertret, "A structured model for simulation of cultures of the cyanobacterium *Spirulina platensis* in photobioreactors: II. Identification of kinetic parameters under light and mineral limitations", *Biotechnology and Bioengineering*, vol. 40, pp. 826–834, 1992.

[12] J.F. Cornet, C.G. Dussap, J.B. Gross, C. Binois, and C. Lasseur, "A simplified monodimensional approach for modeling coupling between radiant light transfer and growth kinetics in photobioreactors", *Chemical Engineering Science*, vol. 50, pp. 1489–1500, 1995.

[13] A. Melis, L. Zhang, M. Forestier, M.L. Ghirardi, and M. Seibert, "Sustained photobiological hydrogen gas production upon reversible inactivation of oxygen evolution in the green alga C*hlamydomonas reinhardtii*", *Plant Physiology*, vol. 117, pp. 129–139, 2000.

[14] H. Berberoğlu, J. Yin, and L. Pilon, "Simulating light transfer in a bubble sparged photobioreactor for simultaneous hydrogen fuel production and CO_2 mitigation", *International Journal of Hydrogen Energy*, vol. 32, pp. 2273–2285, 2007.

[15] M. F. Modest, *Radiative Heat Transfer*, Academic Press, San Diego, CA, 2003.

[16] D. Stramski and C.D. Mobley, "Effect of microbial particles on oceanic optics: a database of single-particle optical properties", *Limnology and Oceanography*, vol. 42, pp. 538–549, 1997.

[17] R.J. Davies-Colley, R.D. Pridmore, and J.E. Hewitt, "Optical properties and reflectance spectra of 3 shallow lakes obtained from a spctrophotometric study", *New Zealand Journal of Marine and Freshwater Research*, vol. 17, pp. 445–459, 1983.

[18] A. Bricaud, A. Morel, and L. Prieur, "Optical efficiency factors of some phytoplankters", *Limnology and Oceanography*, vol. 28, pp. 816–832, 1983.

[19] J.E. Polle, S.D. Kanakagiri, and A. Melis, "tla1, a DNA insertional transformant of the green alga *Chlamydomonas reinhardtii* with a truncated light-harvesting chlorophyll antenna size", *Planta*, vol. 217, pp. 49–59, 2003.

[20] J.E.W. Polle, J.R. Benemann, A. Tanaka, and A Melis, "Photosynthetic apparatus organization and function in the wild type and a chloropyll *b*-less mutant of *Chlamydomonas reinhardtii*. dependence on carbon source", *Planta*, vol. 211, pp. 335–344, 2000.

[21] B. Ke, *Photosynthesis, Photobiochemistry and Photobiophysics*, Kluwer Academic Publishers, Dordrecht, The Netherlands, 2001.

[22] K.G. Privoznik, K.J. Daniel, and F.P. Incropera, "Absorption,extinction, and phase function measurements for algal suspensions of *Chlorella pyrenoidosa*", *Journal of Quantitative Spectroscopy and Radiation Transfer*, vol. 20, pp. 345–352, 1978.

[23] C.F. Bohren, "Multiple scattering of light and some of its observable consequences", *American Journal of Physics*, vol. 55, pp. 524–533, 1986.

[24] M. Jonasz and G.R. Fournier, *Light Scattering by Particles in Water: Theoretical and Experimental Foundations*, Academic Press, San Diego, CA, 2007.

[25] C.F. Bohren and D.R. Huffman, *Absorption and scattering of light by small particles*, John Wiley & Sons, New York, NY, 1998.

[26] K.J. Daniel and F.P. Incropera, "Optical property measurements in suspensions of unicellular algae", Purdue University Technical Report, HTL 77-4, 1977.

[27] C. Moore, R.V. Zeneveld, and J.C. Kitchen, "Preliminary results from an *in situ* spectral absorption meter", Ocean Optics 11, Proceedings of SPIE, vol.1750, pp.330-337, 1992.

[28] J.R.V. Zaneveld, R. Bartz, and J.C. Kitchen, "Reflective tube absorption meter", Ocean Optics 11, Proceedings of SPIE, vol.1302, pp.124-136, 1990.

[29] R.A. Maffione, K.J. Voss, and R.C. Honey, "Measurement of the spectral absorption coefficient in the ocean with an isotropic source", *Applied Optics*, vol. 32, pp. 3273–3279, 1993.

[30] E.S. Fry, G.W. Kattawar, and R.M. Pope, "Integrating cavity absorption meter", *Applied Optics*, vol. 31, pp. 2055–2065, 1992.

[31] G.T. Bennet, E.S. Fry, and F.M. Sogandares, "Photothermal measurements of the absorption coefficient of water at 590 nm", Ocean Optics 8, Proceedings of SPIE, vol.637, pp.172-180, 1986.

[32] R.J. Davies-Colley, R.D. Pridmore, and J.E. Hewitt, "Optical properties of some freshwater phytoplanktonic algae", *Hydrobiologia*, vol. 133, pp. 165–178, 1986.

[33] D. Stramski and J. Piskozub, "Estimation of scattering error in spectrophotometric measurements of light absorption by aquatic particles from three-dimensional radiative transfer simulations.", *Applied Optics*, vol. 42, pp. 3634–3646, 2003.

[34] M.N. Merzlyak and K.R. Naqvi, "On recording the true absorption spectrum and scattering spectrum of a turbid sample: application to cell suspensions of cyanobacterium *Anabaena variabilis*", *Journal of Photochemistry and Photobiology B*, vol. 58, pp. 123–129, 2000.

[35] EH Harris, *The Chlamyydomonas Sourcebook*, Academic Press, New York, NY, 1989.

[36] J.P. Robinson, *Current Protocols in Cytometry*, John Wiley & Sons, New York, NY, 2001.

[37] H.C. Chen and A. Melis, "Localization and function of SulP, a nuclear-encoded chloroplast sulfate permease in *Chlamydomonas reinhardtii*", *Planta*, vol. 220, pp. 198–210, 2004.

[38] W.S. Rasband, "ImageJ", U.S. National Institute of Health, Bethesda, Maryland, USA, http://rsb.info.nih.gov/ij/, 1997-2007.

[39] J.H. Yoon, S.J. Sim, M.S. Kim, and T.H. Park, "High cell density culture of *Anabaena variabilis* using repeated injections of carbon dioxide for the production of hydrogen", *International Journal of Hydrogen Energy*, vol. 27, pp. 1265–1270, 2002.

[40] H. Berberoğlu and L. Pilon, "Experimental measurement of the radiation characteristics of *Anabaena variabilis* ATCC 29413-U and *Rhodobacter sphaeroides* ATCC 49419", *International Journal of Hydrogen Energy*, vol. 32, pp. 4772–4785, 2007.

[41] A.A. Kokhanovsky, "Scattered light corrections to sun photometry: Analytical results for single and multiple scattering regimes", *Journal of Optical Society of America A*, vol. 24, pp. 1131–1137, 2007.

[42] B.M. Agrawal and M.P. Mengüç, "Forward and inverse analysis of single and multiple scattering of collimated radiation in an axisymmetric system", *International Journal of Heat and Mass Transfer*, vol. 34, pp. 633–647, 1991.

[43] V.P. Nicolau, M. Raynaud, and J.F. Sacadura, "Spectral radiative properties identification of fiber insulating materials", *International Journal of Heat and Mass Transfer*, vol. 37, pp. 331–324, 1994.